Heliyon 11 (2025) e40870

Contents lists available at ScienceDirect

Heliyon

journal homepage: www.cell.com/heliyon

Research article

Identification of lethality-related m7G methylation modification patterns and the regulatory features of immune microenvironment in sepsis

Dan Wang *, Rujie Huo, Lu Ye

Department of Respiratory Medicine, The Second Hospital of Shanxi Medical University, 382 Wuyi Road, Xinghualing Area, 030000, Taiyuan, China

ARTICLE INFO

Keywords:
Sepsis
N7-methylguanosine
Diagnostic model
Immune

ABSTRACT

Objectives: N7-methylguanosine (m7G) modification is closely related to the occurrence of human diseases, but its roles in sepsis remain unclear. This study aimed to explore the patterns of lethality-related m7G regulatory factor-mediated RNA methylation modification and immune microenvironment regulatory features in sepsis.

Methods: Three sepsis-related datasets (E-MTAB-4421 and E-MTAB-4451 as training sets and GSE185263 as a validation set) were collected, and differentially expressed m7G-related genes were analyzed between survivors and non-survivors. Lethality-related m7G signature genes were then screened using machine learning methods, followed by the construction of a survival recognition model. Additionally, differences in immune cell distribution were determined and differentially expressed genes (DEGs) between different subtypes were analyzed. Weighted gene co-expression network analysis (WGCNA) was used to select important modules and related hub genes.

Results: In total, 10 differentially expressed m7G-related genes were identified between the survivors and non-survivors, and after further analysis, *EIF4G3*, *EIF4E3*, *NSUN2*, *NUDT4*, and *GEMIN5* were identified as the optimal lethality-related m7G genes. A survival status diagnostic model was then constructed with a combined AUC of 0.678. Fifteen types of immune cells were significantly different between survivors and non-survivors. Sepsis samples were classified into two subtypes, with 22 types of immune cells showing significant differences. Subsequently, 1707 DEGs were identified between the two subtypes, which were significantly enriched in 91 GO terms and 16 KEGG pathways. Finally, the green module with $|\text{correlation}| > 0.3$ was found to be closely related to the subtypes and survival status; further, the top10 hub genes were obtained.

Conclusion: The constructed survival status diagnostic model based on the five lethality-related m7G signature genes may help predict the survival status of patients, and the 10 hub genes obtained may be potential therapeutic targets for sepsis.

1. Introduction

Sepsis is a rapidly worsening systemic disease characterized by multiorgan dysfunction due to a dysregulated inflammatory response to infection [1]. Sepsis is a leading cause of death worldwide, with a mortality rate of 26 % and approximately 20 million

* Corresponding author.
E-mail address: wswjg621@163.com (D. Wang).

https://doi.org/10.1016/j.heliyon.2024.e40870
Received 4 February 2024; Received in revised form 30 November 2024; Accepted 1 December 2024
Available online 4 December 2024

people diagnosed annually. Currently, treatment for sepsis includes early combined antibiotics, fluid resuscitation, and symptomatic vasoactive drug treatment. These therapeutic methods improve the patient's symptoms. However, the risk of infection increases with prolonged hospital stay and invasive surgery [2]. Owing to the heterogeneity and complexity of sepsis in terms of its presentation and population, early identification of sepsis remains a clinical challenge [3]. Therefore, exploring the molecular mechanisms and classification of sepsis is essential for its early diagnosis and treatment.

Sepsis is identified and classified based on specific clinical features or biomarkers. Although some biomarkers, such as chemokines, inflammatory cytokines, the complement system, non-coding RNA, and metabolic-related genes, have been identified, a single biomarker in a clinical setting does not effectively support the diagnosis of sepsis [4,5]. RNA methylation is an abundant RNA modification process in prokaryotes and eukaryotes [6]. N7-methylguanosine (m7G) methylation is one of the most common base modifications involved in post-transcriptional regulation [7]. Recently, RNA methylation, particularly of N6-methyladenosine, was suggested to be involved in the pathogenesis of sepsis [8,9]. Increasing evidence indicates that the m7G modification is closely associated with the occurrence of human diseases [10]. Dai et al. [11] reported that m7G tRNA modification and its methyltransferase complex components, METTL1 and WDR4, are significantly upregulated in intrahepatic cholangiocarcinoma and are closely associated with poor prognosis, indicating that m7G modification is involved in oncogenic mRNA translation and cancer progression. Another study indicates that the tRNA m7G methyltransferase complex proteins METTL1 and WDR4 are significantly upregulated in esophageal squamous cell carcinoma (ESCC), and are related to poor prognosis in ESCC. In addition, N7-methylguanosine tRNA modification promotes ESCC tumorigenesis via the RPTOR/ULK1/autophagy axis [12]. However, systematic investigations on the role of m7G in sepsis remain inadequate.

In the present study, we explored the roles and potential molecular mechanisms of m7G-related genes in sepsis. First, the sepsis expression profile samples were integrated, and differentially expressed m7G-related genes were analyzed between survivors and non-survivors. The optimal m7G-related signature genes were the screened using machine learning methods, and a survival recognition model was constructed using these signature genes; the efficiency of the constructed model was then evaluated. Moreover, sepsis samples were classified into different subtypes according to optimal m7G-related genes, and their correlation with the immune microenvironment was analyzed. Finally, differentially expressed genes (DEGs) between different subtypes were analyzed, and weighted gene co-expression network analysis (WGCNA) was used to select important modules and related hub genes. These results are expected to improve our understanding of the m7G-related mechanisms in sepsis.

2. Materials and methods

2.1. Data collection

Datasets were downloaded from the EBI ArrayExpress database [13]:

A. E-MTAB-4421 included 265 blood samples from patients with sepsis. These included 207 samples from surviving patients and 58 samples from patients who died of sepsis. The detection platform was an Illumina HumanHT-12_V4.
B. E-MTAB-4451 included 106 blood samples from patients with sepsis. These included 56 samples from surviving patients and 50 samples from patients who died of sepsis. The detection platform was an Illumina HumanHT-12_V4.

The two datasets were used as training sets. Using the sva package 3.38.0 [14] in R4.1.2, the combined expression profile data were obtained to remove the batch effect on the expression profile data.

Meanwhile, the expression profile data of GSE185263 [15] were downloaded from the National Center for Biotechnology Information Gene Expression Omnibus database [16]. This study included 345 blood samples obtained from patients with sepsis. Among these, 293 were from surviving patients, whereas 52 were from patients with sepsis who died. The detection platform was an Illumina HiSeq 2500.

2.2. Lethality-related m7G gene screening

First, 29 m7G-related genes were identified from previous studies [17]. The combined samples were then divided into non-survivor and survivor groups. Limma 3.34.7 [18] was used to select the m7G genes with significantly different expression levels between the two groups. The screening threshold was a false discovery rate (FDR) less than 0.05. The expression level correlation between the differentially expressed m7G genes was then calculated using the COR function in R3.6.1.

2.3. Screening of important lethality-related m7G genes by machine learning

Using the combined dataset samples as the training set, three different optimization algorithms were applied to screen for signature genes from the differentially expressed m7G genes. Lars 1.2 [19], caret 6.0-76 [20], and randomForest 4.6-14 [21] were used to perform the least absolute shrinkage and selection operator (LASSO), recursive feature elimination (RFE), and random forest (RF) analyses. The overlapping genes of the three algorithms were selected as the optimal m7G gene combinations.

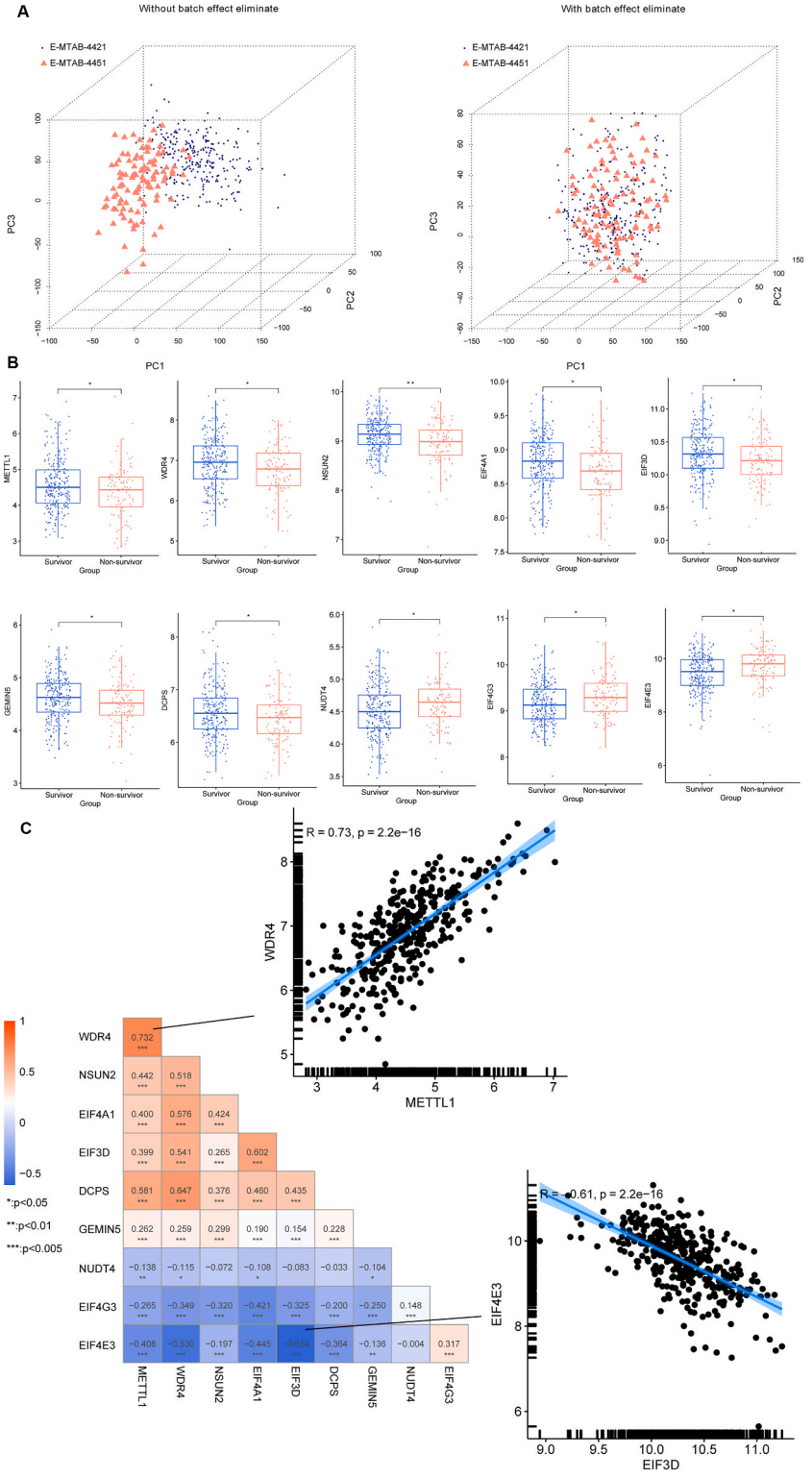

Fig. 1. Lethality-related m7G gene screening.
A. Sample distribution based on gene expression levels before (left panel) and after (right panel) removal of batch effects. B. Expression level distribution of 10 significantly differentially expressed m7G genes. C. Correlation of expression levels between significantly differentially expressed m7G genes.

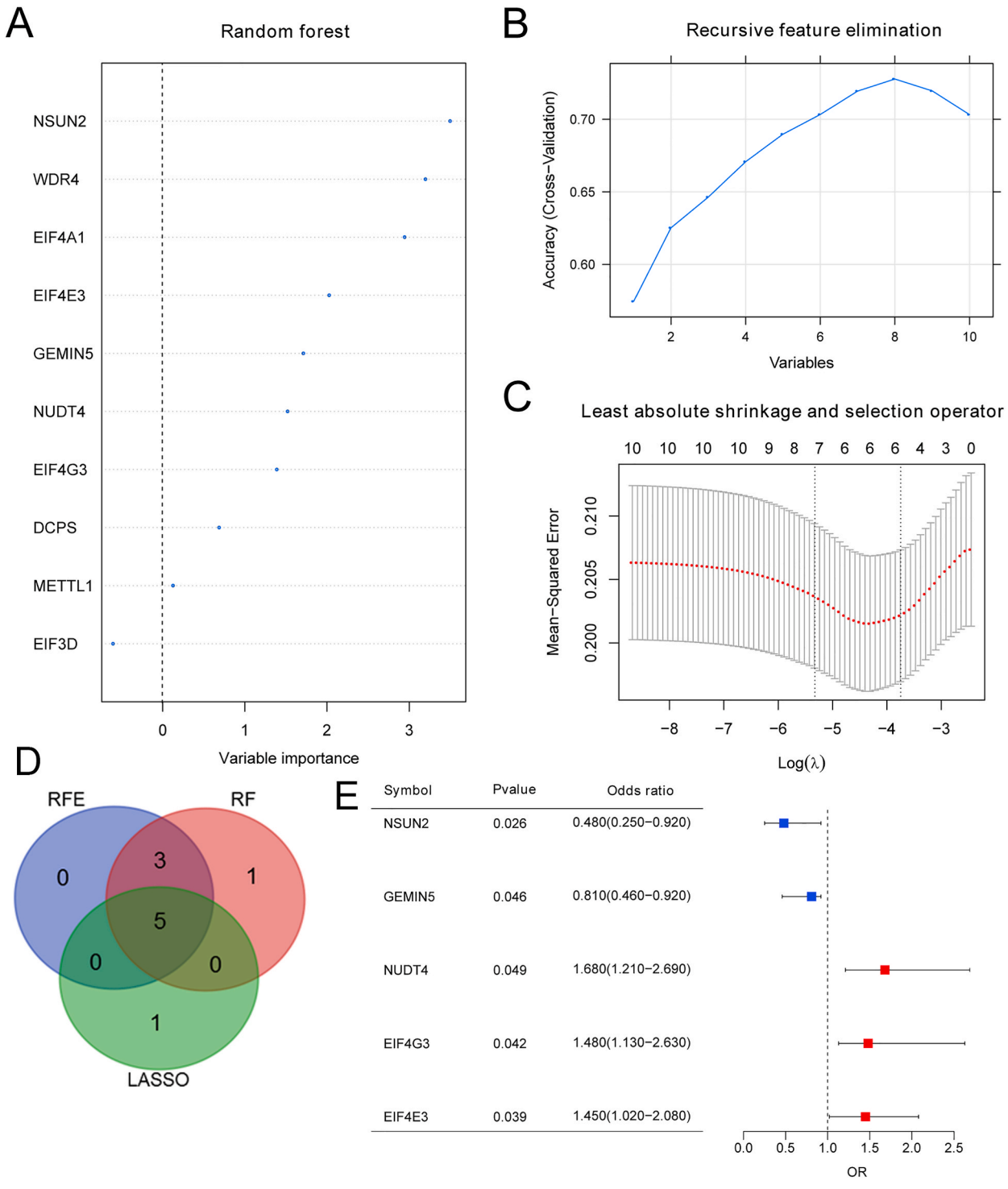

Fig. 2. Screening of important lethality-related m7G gene by machine learning.
A-C. Parameter maps of the RF (A), RF (B), and LASSO algorithms (C) used for m7G signature gene screening. D. Venn diagram of the m7G genes obtained using the three algorithms. E. Multivariate regression analysis of the five optimized genes.

2.4. Construction of the survival state diagnostic model

Based on the expression levels of the optimized m7G genes screened in the training set, the Support Vector Machine [22] in R3.6.1 e1071 1.6-8 was used to construct a sample survival state diagnostic classification system. The receiver operating characteristic (ROC) curve method in pROC 1.12.1 [23] was used to evaluate the performance of the classifier in the training and GSE185263 validation datasets. Finally, RMS 6.3-0 [24] was used to establish a nomogram based on the optimized m7G genes, and a calibration curve was drawn.

2.5. Immune microenvironment analysis

Gene set variation analysis (GSVA 1.36.3) [25], based on a single-sample gene set enrichment analysis algorithm was used to assess the proportion of immune cells in the combined dataset samples. The Kruskal-Wallis test was used to determine differences between the non-survivor and survivor groups. The correlation between the m7G model gene expression level and the difference in immune cells was calculated.

2.6. Unsupervised cluster analysis based on m7G modification model

The expression levels of m7G genes were used to construct a combined model. Subsequently, sample subtype analysis was performed using R3.6.1 ConsensusClusterPlus 1.54.0 [26]. Based on the immune cell proportion results, the distribution differences in the immune cell proportions among the different subtypes were compared using the Kruskal-Wallis test. All Kyoto Encyclopedia of Genes and Genomes (KEGG) signaling pathways and their genes were downloaded from the GSEA MSigDB [27], and the GSVA 1.36.3 [25] algorithm was used to evaluate the quantitative results for each KEGG signaling pathway. The Kruskal-Wallis test was used to quantify the distribution differences of KEGG pathways between the different subtypes.

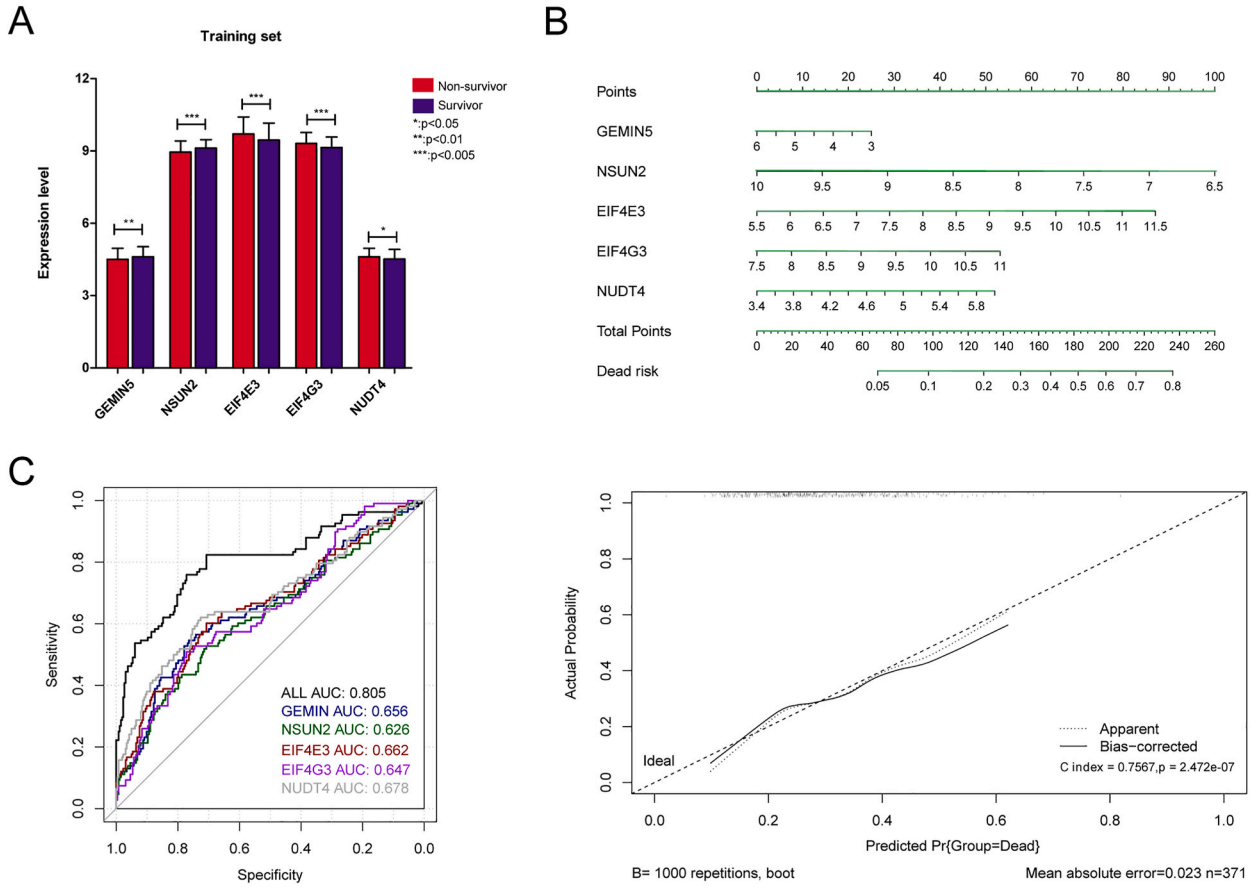

Fig. 3. Construction of survival state diagnostic model.
A. Expression levels of five optimized m7G genes in different survival status groups. B. Nomogram and line chart. C. Receiver operating characteristic curves based on the five optimized m7G genes.

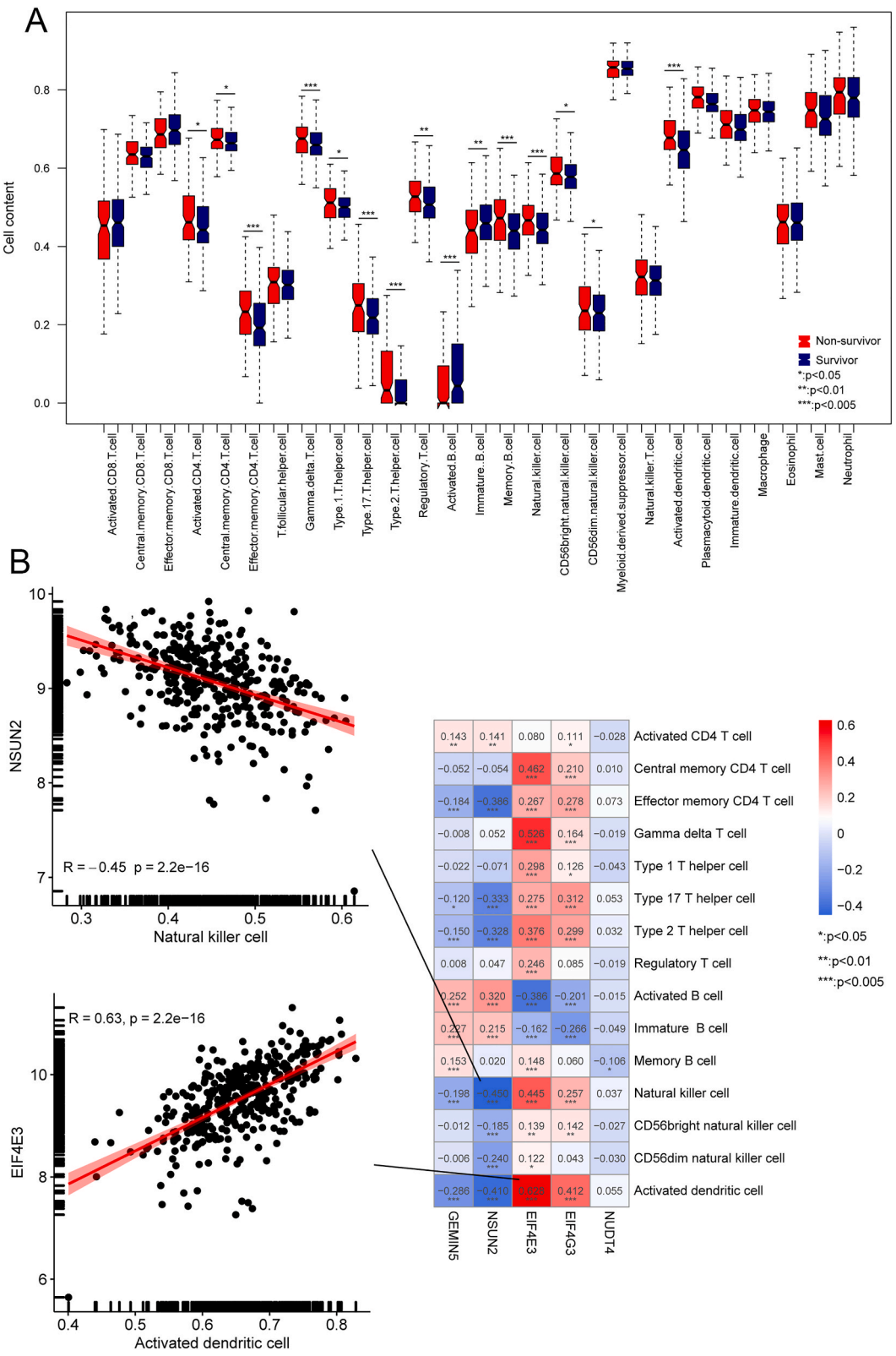

Fig. 4. Immune microenvironment analysis.
Heat map of the distribution of immune cell types. B. Correlation between the five optimized m7G gene expression levels and 15 immune cells with significantly different distributions.

2.7. Screening of significantly differentially expressed genes (DEGs) among different subtypes

In the combined datasets, limma 3.34.7 was used to screen the DEGs between groups with an FDR <0.05 and |Log2FC| > 0.5. DAVID 6.8 [28] was used to analyze the gene ontology (GO) and KEGG pathways of the screened DEGs, with an FDR <0.05 as the threshold.

2.8. Key modules and genes screened by weighted gene co-expression network analysis (WGCNA)

Based on the screened DEGs, the WGCNA 1.61 package [29] in R4.3.1 was utilized to screen the modules related to survival status and subtype grouping. The WGCNA algorithm was executed according to the steps for defining the adjacency function and module partitioning. Module partitioning was performed such that the module set contained at least 50 DEGs with a cut height of 0.995. Modules with a significant |correlation| greater than 0.3, survival status, and subtype grouping were retained. The genes contained in the modules were identified as hub genes, and a co-expression network centered on the hub genes was constructed.

3. Results

3.1. Lethality-related m7G gene screening

First, the two datasets were merged into a single dataset by removing batch effects. In total, 371 samples were obtained. These included 263 survivor samples and 108 non-survivor samples. The distribution of samples based on gene expression levels before and after removing batch effects is shown in Fig. 1A. Then, 29 m7G genes were collected from previous studies and their expression levels of m7G genes were extracted from the combined samples. The 10 m7G genes with significant differential expression between the non-survivor and survivor groups were screened under an FDR less than 0.05 (Fig. 1B). The correlation between the expression levels of the 10 m7G genes is shown in Fig. 1C.

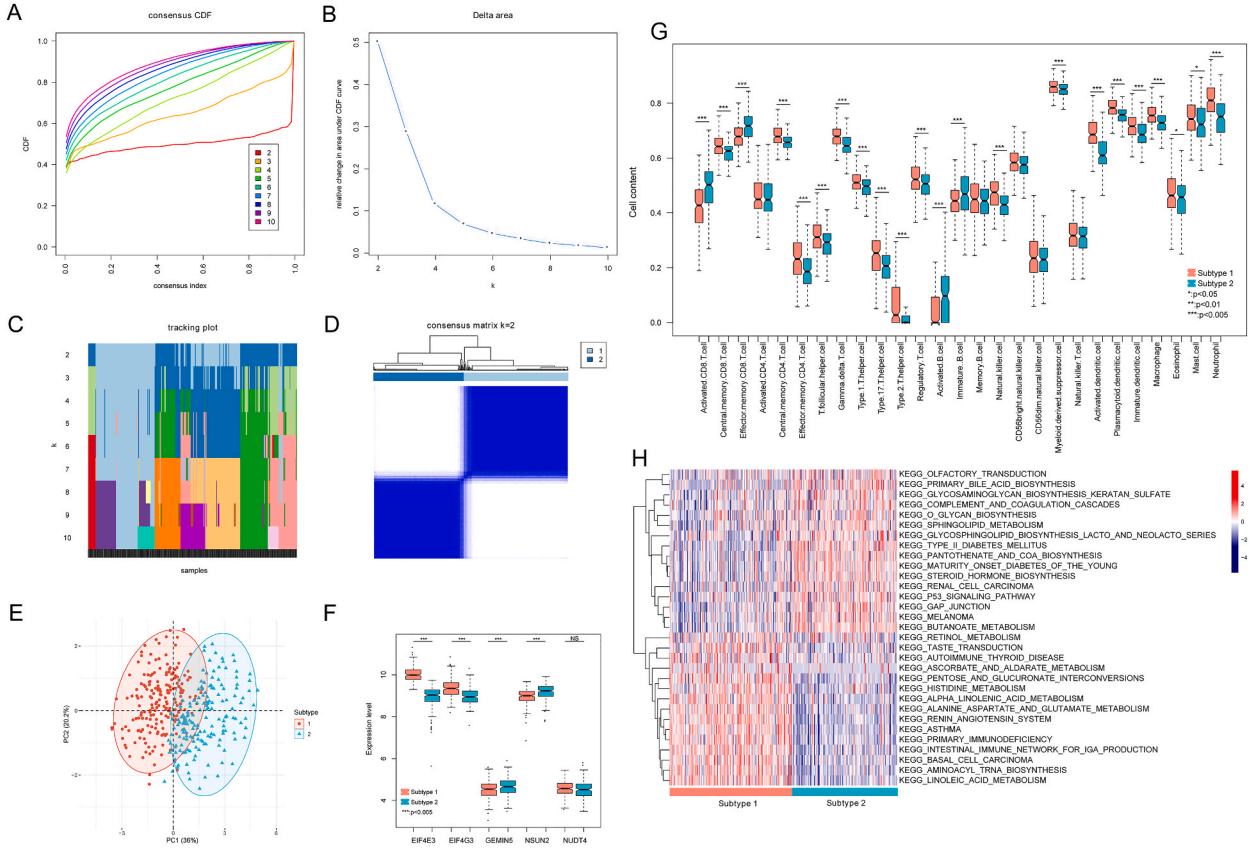

Fig. 5. Unsupervised cluster analysis based on m7G modification model.
A-D. Presentation of parameters and results for subtyping samples based on five m7G genes. E. Identification of different sample subtypes based on the five m7G genes. F. Distribution of the expression levels of the five m7G genes in the two subtypes. G. Distribution of immune cells into different subtypes. H. Kyoto Encyclopedia of Genes and Genomes (KEGG) signaling pathways showed significantly different distributions in different subtypes.

3.2. Screening of important lethality-related m7G genes by machine learning

The LASSO, RFE, and RF algorithms yielded six, eight, and nine m7G genes, respectively (Fig. 2A–C). The Venn analysis identified five overlapping genes: *EIF4G3*, *EIF4E3*, *NSUN2*, *NUDT4*, and *GEMIN5* (Fig. 2D). The five m7G genes were considered as the optimized

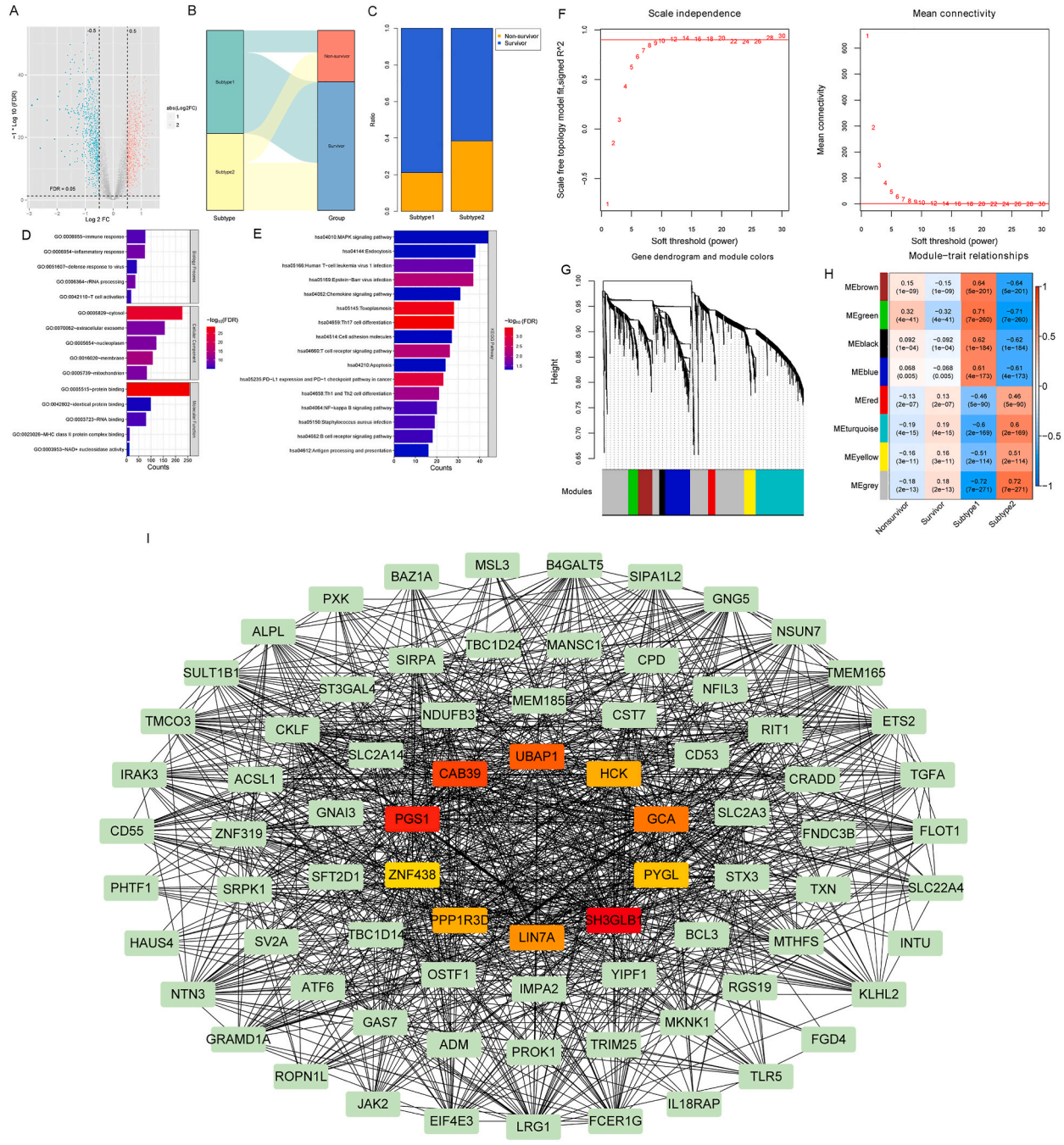

Fig. 6. Hub gene identification.
A. Volcano plot for the differential expression analysis (blue and red dots indicate significantly downregulated and upregulated genes, respectively). B. Sankey plots corresponding to samples grouped by different subtypes and with different survival statuses. C. Distribution of samples with different survival statuses in different subtypes. D and E. Gene ontology (D) and KEGG (E) signaling pathways enriched in differentially expressed genes. F. Left: Selection diagram of the adjacency matrix weight parameter (power); Right: Average connectivity of genes under different power parameters. G. Module partition tree diagram, where each color indicates a different module. H. Module-trait correlation heatmap. I. The Co-expression network centered on hub genes in the green module.

m7G gene combination. The results of the multifactor regression analysis of the five genes are shown in Fig. 2E.

3.3. Construction of survival state diagnostic model

In the combined dataset and GSE185263 independent validation dataset, the survival status diagnosis classification model of the samples was constructed according to the five optimized m7G gene expression levels (Fig. 3A and S1A). An ROC curve was then drawn to evaluate model efficacy. As shown in Fig. 3B and S1B, the model was highly sensitive and specific based on the AUC values. Finally, a nomogram model was constructed and a broken-line analysis was performed for the two datasets. Based on this, the nomogram showed a greater predictive power (Fig. 3C and S1C).

3.4. Immune microenvironment analysis

The proportions of the 28 immune cell types were determined based on the gene expression profile data of the combined dataset samples. Differences in the distribution of these immune cells across different survival statuses were then compared. Fifteen immune cell types were screened for significant differences between groups. These included activated CD4 T cells, type 2 T helper cells, memory B cells, activated B cells, immature B cells, natural killer cells, CD56dim natural killer cells, CD56bright natural killer cells, and activated dendritic cells (Fig. 4A). Next, the correlation between the expression of *EIF4G3*, *EIF4E3*, *NSUN2*, *NUDT4*, and *GEMIN5* and the 15 immune cells with significantly different distributions was calculated (Fig. 4B). *NSUN2* showed the strongest negative correlation with natural killer cells. *EIF4E3* showed the strongest positive correlation with activated dendritic cells.

3.5. Unsupervised cluster analysis based on m7G modification model

Based on the expression levels of the five m7G genes in the combined samples, the combined samples were divided into two subtypes consisting of 199 and 172 samples, respectively (Fig. 5A–D). Principal component analysis (PCA) of the sample distribution was conducted for the two subtypes. The samples from the two subtypes were clearly distinguishable (Fig. 5E). In addition, a comparative analysis was conducted based on the expression distribution of the five m7G genes in the two subtypes. As presented in Fig. 5F, the expression levels of *EIF4G3*, *EIF4E3*, *NSUN2*, and *GEMIN5* differed significantly between the two subtypes. Subsequently, based on the proportion of immune cells, the distribution differences in immune cells between different subtypes were analyzed. As shown in Fig. 5G, 22 immune cell types were identified. These cells include central memory CD8 + T cells, activated CD8 + T cells, immature B cells, natural killer cells, macrophages, and neutrophils. Moreover, 31 KEGG signaling pathways with significant differences in their distribution were screened. These included olfactory transduction, primary bile acid biosynthesis, and the p53 signaling pathway (Fig. 5H).

3.6. DEG selection between two subtypes

In total, 1707 DEGs were identified between the two subtypes (Fig. 6A). Moreover, samples from different survival states in different subtypes were analyzed. As shown in Fig. 6B and C, subtype 1 included 73 non-survivor and 126 survivor samples, whereas subtype 2 included 35 non-survivor and 137 survivor samples. The Chi-square test indicated that the distribution of non-survivor samples in subtype 1 was significantly higher than that in subtype 2 ($p = 0.0005811$).

GO and KEGG pathway analyses of the screened significant DEGs identified 19 biological processes (such as immune response and inflammatory response), 47 cellular components, nine molecular functions, and 16 pathways (such as MAPK signaling pathway and chemokine signaling pathway) (Fig. 6D and E).

3.7. Key modules and genes screening by WGCNA

To satisfy the premise of a scale-free network distribution, the power value was selected when the square value of the correlation coefficient reached 0.9 for the first time (power = 12) (Fig. 6F). The dissimilarity coefficient between the nodes was then calculated, and a system clustering tree was obtained. Eight modules were identified (Fig. 6G). Correlations among the module, subtype, and survival state were calculated, and the results are shown in Fig. 6H. The module with |correlation| greater than 0.3 was retained. The green module, containing 83 genes, was finally selected. The topGenesKME algorithm in the WGCNA algorithm was used to identify the top 10 hub genes in the green module, and a co-expression network was created using these genes as the center (Fig. 6I).

4. Discussion

Despite continuous investigation of sepsis, its morbidity and mortality have increased. The identification of novel biomarkers is important for early diagnosis and treatment. Moreover, owing to significant heterogeneity among patients, identification of distinct molecular subtypes is also critical [30]. In this study, five lethality-related m7G genes (*EIF4G3*, *EIF4E3*, *NSUN2*, *NUDT4*, and *GEMIN5*) were identified via machine learning methods, and a survival status diagnostic model was constructed. Based on these signature genes, the sepsis samples were classified into two subtypes. The immune microenvironment and pathway distribution differed significantly between the two subtypes.

Epigenetic alterations refer to gene expression changes in response to external stimuli and reportedly play a critical role in the

pathogenesis of sepsis [31]. One type of epigenetic regulation, m7G methylation, is involved in multiple human diseases [32]; however, its role in sepsis has rarely been discussed [33]. In the present study, which focused on lethality-related m7G genes, we identified five m7G genes (*EIF4G3*, *EIF4E3*, *NSUN2*, *NUDT4*, and *GEMIN5*) in sepsis samples using machine learning methods, suggesting an association between m7G methylation and sepsis. A previous study found that *NUDT4* and PARN are key genes in sepsis, and real-time quantitative PCR confirmed the upregulation of *NUDT4* in patients with sepsis [33]. Further, *EIF4G3*, *EIF4E3*, *NSUN2*, and *GEMIN5* have not been reported in sepsis but are closely associated with human cancer prognoses. For example, *EIF4G3* was identified as a prognostic gene for sarcoma associated with m7G [34], and higher expression of *EIF4E3* related to m7G indicated a good prognosis and could significantly influence the biological behavior of osteosarcoma cells. Hu et al. [35] demonstrated that SUMO-2/3-modified *NSUN2* could promote gastric cancer progression and regulate mRNA m5C methylation, indicating that *NSUN2* may be a potential target for gastric cancer. Another study used *EIF4E3*, *GEMIN5*, and *NCBP2* to establish an m7G risk score (MRS) model for assessing the prognosis of colorectal cancer, indicating that *EIF4E3*, *GEMIN5*, and *NCBP2* may be targets for the prognosis of colorectal cancer [36]. Furthermore, based on these five m7G-related genes, a survival state diagnostic model was constructed, and the receiver operating characteristic (ROC) curve revealed that the model was sensitive and specific, depending on the AUC values (0.678). The nomogram also showed that the model had an ideal predictive power. In a previous study, Lu et al. identified six disease characteristic genes, including *NUDT4B*, *IFIT5*, *LARP1*, *EIF4E*, *LSM1*, and *NUDT4*, using machine learning methods, and built a nomogram model based on these six genes, which could be used to accurately assess the risk of COVID-19 [37]. Another study also proposed an m7G-related prediction model for lung adenocarcinoma (LUAD) based on EIF3D, EIF4E, NCBP1, and NCBP2 and observed that the AUC values for 1-year, 3-year, and 5-year survival were 0.737, 0.736, and 0.731, respectively, implying that the model performs well in predicting the survival of patients with LUAD [38]. Taken together, *EIF4G3*, *EIF4E3*, *NSUN2*, *NUDT4*, and *GEMIN5* associated with m7G may be used as potential targets for the survival of patients with sepsis, and the proposed survival state diagnostic model may be used for predicting sepsis survival. Owing to the heterogeneity of sepsis, a subgroup analysis was performed. Based on the five m7G-related genes, the sepsis samples were divided into two subtypes. Immune cell infiltration analysis revealed 22 immune cell types with distribution differences between the two subtypes. Of these immune cell types, 11 were T cells. The proportions of immune cells in the groups with different survival statuses were also compared. Fifteen cell types with eight T cells were identified. Sepsis is characterized by an imbalance between immunosuppression and hyperinflammation [39]. Sepsis affects the immune system by altering the production and function of effector cells responsible for homeostasis [40]. Aberrant $CD8^+$ T cell, $CD4^+$ T cell, and regulatory T cell responses are reportedly involved in sepsis [39]. T cells exhibit prolonged functional impairment during sepsis [41]. Based on the results of the present study, improving T cell activity in patients with sepsis may help in the development of new treatment options for sepsis.

Further, DEGs involved in inflammatory and immunological functions and pathways between the two subtypes were selected. These DEGs were involved in the immune response, inflammatory response, and chemokine signaling pathways, consistent with the inflammatory features of sepsis. The distribution of non-survivors in subtype 1 was higher than that in subtype 2, suggesting a better prognosis for subtype 2. Based on these DEGs, ten hub genes were selected using WGCNA. In the co-expression network centered on hub genes, a model gene (*EIF4E3*), which was co-expressed with seven of the ten hub genes (*CAB39*, *GCA*, *PGS1*, *UBAP1*, *LIN7A*, *SH3GLB1*, and *PPP1R3D*), was included. *PGS1* and *SH3GLB1* have been reported as hub genes in pediatric sepsis [42]. Therefore, these hub genes may serve as potential therapeutic targets for sepsis.

However, this study has some limitations. First, the specific roles and underlying mechanisms of the identified m7G-related genes, modules determined by WGCNA, hub genes, and enriched pathways in sepsis should be further investigated using *in vitro* and *in vivo* experiments. Secondly, potential biases, confounders, and uncontrolled variables should be considered. Third, specific mechanistic insights into immune cells and the dynamic nature of immune responses during sepsis should be investigated using various experiments. Additionally, the clinical heterogeneity of sepsis warrants further evaluation and the clinical applicability of the proposed survival diagnostic model for sepsis needs to be verified using a large number of clinical samples.

5. Conclusions

In conclusion, we established a survival status diagnostic model based on five lethality-related m7G genes. This model may aid in the prediction of patient survival. Additionally, the sepsis samples were classified into two subtypes, further suggesting the heterogeneity of sepsis. Significantly different immune microenvironments were observed across groups with different survival statuses and between the two subtypes. Furthermore, ten hub genes were identified as potential therapeutic targets for sepsis. Overall, the findings of the present study contribute to a better understanding of sepsis progression.

CRediT authorship contribution statement

Dan Wang: Writing – review & editing, Writing – original draft. **Rujie Huo:** Formal analysis, Data curation. **Lu Ye:** Software, Data curation.

Ethics approval and consent to participate

Not applicable.

Data availability statement

The data analyzed in this study were obtained from the EBI ArrayExpress database (https://www.ebi.ac.uk/biostudies/arrayexpress) with accession numbers E-MTAB-4421 and E-MTAB-4451 and Gene Expression Omnibus (accession number GSE185263).

Funding statement

This study received no additional funding support.

Declaration of competing interest

The authors declare that they have no known competing financial interests or personal relationships that could have appeared to influence the work reported in this paper.

Acknowledgments

The authors would like to thank all the staff members of the Department of Respiratory Medicine at the Second Hospital of Shanxi Medical University. The authors sincerely thank Dr. Rujie Huo for her contribution to the conception and design of this study. The authors acknowledge Mrs. Lu Ye, who performed the data analysis and provided technical assistance. The authors declare no potential conflicts of interest.

Appendix A. Supplementary data

Supplementary data to this article can be found online at https://doi.org/10.1016/j.heliyon.2024.e40870.

References

[1] M. Singer, et al., The third international consensus definitions for sepsis and septic shock (Sepsis-3), JAMA 315 (8) (2016) 801–810.
[2] Y.Y. Zhang, B.T. Ning, Signaling pathways and intervention therapies in sepsis, Signal Transduct. Targeted Ther. 6 (1) (2021) 21–816.
[3] H.J. de Grooth, et al., Unexplained mortality differences between septic shock trials: a systematic analysis of population characteristics and control-group mortality rates, Intensive Care Med. 44 (3) (2018) 311–322.
[4] T. Barichello, et al., Biomarkers for sepsis: more than just fever and leukocytosis-a narrative review, Crit. Care 26 (1) (2022) 21–3862.
[5] D. Yang, et al., CircRNA_0075723 protects against pneumonia-induced sepsis through inhibiting macrophage pyroptosis by sponging miR-155-5p and regulating SHIP1 expression, Front. Immunol. 14 (2023) 1095457.
[6] H. Shi, J. Wei, C. He, Where, when, and how: context-dependent functions of RNA methylation writers, readers, and erasers, Mol. Cell 74 (4) (2019) 640–650.
[7] X. Zhang, et al., Biological roles of RNA m7G modification and its implications in cancer, Biol. Direct 18 (1) (2023) 23–414.
[8] A. Binnie, et al., Epigenetics of sepsis, Crit. Care Med. 48 (5) (2020) 745–756.
[9] L. Zhu, et al., RNA m6A methylation regulators in sepsis, Mol. Cell. Biochem. 2 (10) (2023) 23–4841.
[10] C. Dai, et al., Iterative feature representation algorithm to improve the predictive performance of N7-methylguanosine sites, Briefings Bioinf. 22 (4) (2021).
[11] Z. Dai, et al., N(7)-Methylguanosine tRNA modification enhances oncogenic mRNA translation and promotes intrahepatic cholangiocarcinoma progression, Mol. Cell 81 (16) (2021) 3339–3355.e8.
[12] H. Han, et al., N(7)-methylguanosine tRNA modification promotes esophageal squamous cell carcinoma tumorigenesis via the RPTOR/ULK1/autophagy axis, Nat. Commun. 13 (1) (2022) 1478.
[13] U. Sarkans, et al., From ArrayExpress to BioStudies, Nucleic Acids Res. 49 (D1) (2021) D1502–D1506.
[14] J.T. Leek, et al., The sva package for removing batch effects and other unwanted variation in high-throughput experiments, Bioinformatics 28 (6) (2012) 882–883.
[15] A. Baghela, et al., Predicting sepsis severity at first clinical presentation: the role of endotypes and mechanistic signatures, EBioMedicine 75 (2022) 103776.
[16] T. Barrett, et al., NCBI GEO: archive for functional genomics data sets–update, Nucleic Acids Res. 41 (Database issue) (2013) 27.
[17] C. Ma, et al., Identification of m(7)G regulator-mediated RNA methylation modification patterns and related immune microenvironment regulation characteristics in heart failure, Clin. Epigenet. 15 (1) (2023) 23–1439.
[18] M.E. Ritchie, et al., limma powers differential expression analyses for RNA-sequencing and microarray studies, Nucleic Acids Res. 43 (7) (2015) 20.
[19] J.J. Goeman, L1 penalized estimation in the Cox proportional hazards model, Biom. J. 52 (1) (2010) 70–84.
[20] T.M. Deist, et al., Machine learning algorithms for outcome prediction in (chemo)radiotherapy: an empirical comparison of classifiers, Med. Phys. 45 (7) (2018) 3449–3459.
[21] L. Tolosi, T. Lengauer, Classification with correlated features: unreliability of feature ranking and solutions, Bioinformatics 27 (14) (2011) 1986–1994.
[22] Q. Wang, X. Liu, Screening of feature genes in distinguishing different types of breast cancer using support vector machine, OncoTargets Ther. 8 (2015) 2311–2317.
[23] X. Robin, et al., pROC: an open-source package for R and S+ to analyze and compare ROC curves, BMC Bioinf. 12 (77) (2011) 1471–2105.
[24] J. Wu, et al., A nomogram for predicting overall survival in patients with low-grade endometrial stromal sarcoma: a population-based analysis, Cancer Commun. 40 (7) (2020) 301–312.
[25] L. Ye, et al., Tumor-infiltrating immune cells act as a marker for prognosis in colorectal cancer, Front. Immunol. 10 (2368) (2019).
[26] X. Zhang, et al., Identification of immune-related lncRNAs in periodontitis reveals regulation network of gene-lncRNA-pathway-immunocyte, Int. Immunopharm. 84 (106600) (2020) 14.
[27] Y. Ye, Q. Dai, H. Qi, A novel defined pyroptosis-related gene signature for predicting the prognosis of ovarian cancer, Cell Death Dis. 7 (1) (2021) 21–451.
[28] W. Huang da, B.T. Sherman, R.A. Lempicki, Systematic and integrative analysis of large gene lists using DAVID bioinformatics resources, Nat. Protoc. 4 (1) (2009) 44–57.
[29] P. Langfelder, S. Horvath, WGCNA: an R package for weighted correlation network analysis, BMC Bioinf. 9 (559) (2008) 1471–2105.

[30] M. Huang, S. Cai, J. Su, The pathogenesis of sepsis and potential therapeutic targets, Int. J. Mol. Sci. 20 (21) (2019).
[31] D. Wu, et al., Epigenetic mechanisms of Immune remodeling in sepsis: targeting histone modification, Cell Death Dis. 14 (2) (2023) 23–5656.
[32] Y. Luo, et al., The potential role of N(7)-methylguanosine (m7G) in cancer, J. Hematol. Oncol. 15 (1) (2022) 22–1285.
[33] J. Gong, et al., Construction of m7G subtype classification on heterogeneity of sepsis, Front. Genet. 13 (2022) 1021770.
[34] H. Qin, et al., Identification and verification of m7G-Related genes as biomarkers for prognosis of sarcoma, Front. Genet. 14 (2023) 1101683.
[35] Y. Hu, et al., NSUN2 modified by SUMO-2/3 promotes gastric cancer progression and regulates mRNA m5C methylation, Cell Death Dis. 12 (9) (2021) 842.
[36] X. Huang, et al., The prognostic index of m(7)G-related genes in CRC correlates with immune infiltration, Sci. Rep. 12 (1) (2022) 21282.
[37] L. Lu, et al., The m7G modification level and immune infiltration characteristics in patients with COVID-19, J. Multidiscip. Healthc. 15 (2022) 2461–2472.
[38] Y. Liu, et al., m7G-related gene NUDT4 as a novel biomarker promoting cancer cell proliferation in lung adenocarcinoma, Front. Oncol. 12 (2022) 1055605.
[39] T. van der Poll, M. Shankar-Hari, W.J. Wiersinga, The immunology of sepsis, Immunity 54 (11) (2021) 2450–2464.
[40] M. Bosmann, P.A. Ward, The inflammatory response in sepsis, Trends Immunol. 34 (3) (2013) 129–136.
[41] I.J. Jensen, et al., Sepsis-Induced T cell immunoparalysis: the ins and outs of impaired T cell immunity, J. Immunol. 200 (5) (2018) 1543–1553.
[42] X. Zhang, et al., Analysis of mRNA-lncRNA and mRNA-lncRNA-pathway co-expression networks based on WGCNA in developing pediatric sepsis, Bioengineered 12 (1) (2021) 1457–1470.